Quantum mechanical modelling of the grain-surface formation of acetaldehyde on H$_2$O:CO dirty ice surfaces

Jessica Perrero,[1,2] Piero Ugliengo [ID],[2] Cecilia Ceccarelli [ID][3] and Albert Rimola [ID][1]⋆

[1]*Departament de Química, Universitat Autònoma de Barcelona, E-08193 Bellaterra, Catalonia, Spain*
[2]*Dipartimento di Chimica and Nanostructured Interfaces and Surfaces (NIS) Centre, Università degli Studi di Torino, via P. Giuria 7, I-10125 Torino, Italy*
[3]*CNRS, Institut de Planétologie et d'Astrophysique de Grenoble (IPAG), Université Grenoble Alpes, F-38000 Grenoble, France*

ABSTRACT

Acetaldehyde (CH$_3$CHO) is one of the most detected interstellar complex organic molecules (iCOMs) in the interstellar medium (ISM). These species have a potential biological relevance, as they can be precursors of more complex species from which life could have emerged. The formation of iCOMs in the ISM is a challenge and a matter of debate, whether gas-phase, grain-surface chemistry, or both are needed for their synthesis. In the gas-phase, CH$_3$CHO can be efficiently synthesized from ethanol and/or ethyl radical. On the grain-surfaces, radical–radical recombinations were traditionally invoked. However, several pitfalls have been recently identified, such as the presence of energy barriers and competitive side reactions (i.e. H abstractions). Here, we investigate a new grain-surface reaction pathway for the formation of acetaldehyde, namely the reaction between CH$_3$ and a CO molecule of a dirty water/CO ice followed by hydrogenation of its product, CH$_3$CO. To this end, we carried out *ab initio* computations of the reaction occurring on an ice composed of 75 per cent water and 25 per cent CO molecules. We found that the CH$_3$ + CO$_{(ice)}$ reaction exhibits barriers difficult to overcome in the ISM, either adopting a Langmuir–Hinshelwood or an Eley–Rideal mechanism. The subsequent hydrogenation step is found to be barrierless, provided that the two reacting species have the correct orientation. Therefore, this pathway seems unlikely to occur in the ISM.

Key words: astrochemistry – molecular processes – ISM: molecules.

1 INTRODUCTION

Acetaldehyde is one of the most common detected interstellar complex organic molecules (iCOMs), which are chemical compounds defined as molecules with six or more atoms that contain at least one carbon atom (Herbst & van Dishoeck 2009; Ceccarelli et al. 2017; Herbst 2017). Since their detection in star-forming regions, iCOMs rose the interest of scientists. There is evidence that some iCOMs formed in the interstellar medium (ISM) were inherited by the small objects of the Solar system (Cazaux et al. 2003; Caselli & Ceccarelli 2012; Ceccarelli et al. 2014; Ligterink et al. 2018; Bianchi et al. 2019; Drozdovskaya et al. 2019). These species, after thermal and hydrothermal alterations, can be converted into more complex organic species (Yabuta et al. 2007; Callahan et al. 2011; Alexander et al. 2014; Rotelli et al. 2016), therefore potentially paving the way to the emergence of life on Earth.

Acetaldehyde was first detected in Sagittarius B2 by Gottlieb (1973), Fourikis et al. (1974), and Gilmore et al. (1976). Some years later, it was also detected in cold clouds, TMC-1 and L134N, by Matthews, Friberg & Irvine (1985). This molecule has been found in a large number of environments: cold pre-stellar cores (Bacmann et al. 2012; Scibelli & Shirley 2020), hot cores (Blake et al. 1987; Law et al. 2021), hot corinos (Cazaux et al. 2003; Chahine et al. 2022), protostellar molecular shocks (Lefloch et al. 2017; De Simone et al.

2020), young discs (Codella et al. 2018; Lee et al. 2019), and also in comets (Crovisier et al. 2004; Biver et al. 2021).

The presence of acetaldehyde (CH$_3$CHO) and other iCOMs in cold pre-stellar cores demonstrates that their synthesis cannot be the result of grain-surface reactions involving migration of species (i.e. radicals) other than H and O (e.g. Bacmann et al. 2012; Ceccarelli et al. 2022).

The reaction pathways that lead to iCOMs are still a matter of debate, as both gas-phase and grain-surface chemistry are invoked to play a crucial role in their synthesis (e.g. Garrod, Weaver & Herbst 2008; Balucani, Ceccarelli & Taquet 2015; Ceccarelli et al. 2022). Several paradigms for the formation of iCOMs were proposed in the literature, the most popular being schemes based on gas-phase reactions (e.g. Charnley, Tielens & Millar 1992; Charnley, Tielens & Rodgers 1997; Balucani et al. 2015; Taquet, Wirström & Charnley 2016; Skouteris et al. 2018; Vazart et al. 2020) and a network of radical–radical couplings occurring on the surface of grains (e.g. Garrod & Herbst 2006; Garrod et al. 2008; Jin & Garrod 2020). Other paradigms include a mechanism based on the condensation of atomic C (Ruaud et al. 2015; Krasnokutski, Jäger & Henning 2020), on the excited O-atom insertion (Bergner, Öberg & Rajappan 2017, 2019), or on the formation of HCO radical on ice surfaces as a parent precursor of other iCOMs (Fedoseev et al. 2015; Simons, Lamberts & Cuppen 2020).

For what concerns acetaldehyde, several works investigated its formation routes from an experimental and theoretical point of view. In the gas-phase, the reaction between ethyl radical and atomic

⋆ E-mail: albert.rimola@uab.cat

oxygen was proposed to yield CH_3CHO by Charnley (2004), as well as the insertion of CH into methanol (Vasyunin et al. 2017). In KIDA (Wakelam et al. 2012) and UMIST (McElroy et al. 2013) data bases, an ionic route involving protonated acetaldehyde (obtained from dimethyl ether) is present. Finally, in 2018, the idea that acetaldehyde (and other iCOMs) can arise from the chemical transformation of ethanol in the gas-phase was proposed (Skouteris et al. 2018). In this chemical network, called the genealogical tree of ethanol, the latter is the precursor (the parent molecule) that give rise to different iCOMs such as glycolaldehyde, acetic acid, formic acid, and acetaldehyde, among others. More recently, Vazart et al. (2020) carried out a systematic study of all gas-phase reactions present in the literature, which lead to the formation of acetaldehyde, and performed new *ab initio* computations for reactions having only guessed product and rate constants. These authors confirmed the pathways starting from ethyl radical (Charnley 2004) and ethanol (Skouteris et al. 2018) and discarded the others (as they used incorrect product or rate constants). In their study, Vazart et al. (2020) also showed that the ethanol genealogical tree is currently the most promising explanation for the synthesis of acetaldehyde in warm objects. Perrero et al. (2022a) proposed that ethanol would be formed on the grain-surface by the reaction of CCH with a water molecule of the ice, followed by hydrogenation of the produced vinyl alcohol. Remarkably, the presence of frozen ethanol has been tentatively detected by *JWST* observations (although needs confirmation) (Yang et al. 2022; McClure et al. 2023), supporting the hypothesis of the ethanol being the mother of acetaldehyde.

On the grain surfaces, experimental results are in some cases contradictory. Acetaldehyde was formed in ices containing H_2O, CO, CH_4, and CH_3OH processed by UV-irradiation (Moore & Hudson 1998; Bennett et al. 2005; Öberg et al. 2009, 2010; Paardekooper, Bossa & Linnartz 2016; Martín-Doménech, Öberg & Rajappan 2020). In the experiments by Chuang et al. (2021), a number of iCOMs were obtained by irradiating with 200 keV H^+ ions $C_2H_2:H_2O$ ices, including acetaldehyde. However, in experiments using a matrix isolation technique of UV-illuminated methanol ices, where the presence of radicals could be monitored, Gutiérrez-Quintanilla et al. (2021) found that several iCOMs were formed, except acetaldehyde. Finally, the experiments by Fedoseev et al. (2022) produced acetaldehyde and its precursor, ketene, via a non-energetic pathway, where CO is co-deposited with C, H, and H_2O at 10 K.

From a theoretical point of view, the radical–radical coupling of HCO and CH_3 was proposed by Garrod & Herbst (2006) to yield CH_3CHO on icy grain surfaces, as it was supposed that the reaction is barrierless due to taking place between two radical species. However, successive studies showed that not only this reaction has an energy barrier (because the radicals are physisorbed on the ice surface and have to break the intermolecular forces with the surface to react), but it also presents a competitive channel leading to the formation of CH_4 + CO (Enrique-Romero et al. 2019, 2020). The same reaction simulated on a model of CO ice gave similar results, culminating in one of these three outcomes: formation of CH_3CHO, H-abstraction yielding CH_4 + CO, or no reaction taking place (Lamberts et al. 2019). A recent study by Enrique-Romero et al. (2021) concluded that the efficiency of acetaldehyde formation via radical coupling is a strong function of the mobility of the radicals on the grain surface (and, consequently, of the grain temperature), in which the easier the diffusion of HCO and CH_3, the less the acetaldehyde formation efficiency. Finally, recent kinetic calculations of Ben Chouikha et al. (2022) on the reaction between atomic carbon and methanol proposed by Singh, Tandon & Misra (2019) show the presence of a slow

reaction step preceding the barrierless formation of acetaldehyde from the radicals HCO and CH_3. However, at low temperature, the product can be formed due to tunnelling effects. We notice, however, that the simultaneous presence of methanol and atomic carbon on the grain-surfaces is unlikely, as methanol is mostly formed by the hydrogenation of frozen CO, i.e. when carbon is prevalently locked into CO.

In summary, there is evidence that, in hot cores/corinos, acetaldehyde is formed in the gas-phase by reactions occurring in the warm gas, but it is still unclear whether this is the only mechanism at work, especially in cold environments. In light of this situation, in this work, we decided to delve into the non-energetic formation of acetaldehyde on the surface of dust grains, when radicals cannot diffuse.

When dealing with surface reactions, several mechanisms can operate: (i) Langmuir–Hinshelwood (LH: Langmuir 1922; Hinshelwood 1930) reactions, which are efficient in the case where one of the reactants can easily diffuse on the surface of the grains (Hasegawa & Herbst 1993); (ii) Eley–Rideal (ER: Eley & Rideal 1940) reactions, in which species from the gas-phase directly react with surface molecules, avoiding diffusion, but are efficient only if there are sufficient reactive species on the grain surface and if the reactions do not possess an activation energy (Ruaud et al. 2015); (iii) Harris–Kasemo hot atom reactions, in which a high-energy species has enough energy to overcome the diffusion barriers and travels on the surface until all excess energy is lost or it reacts (Harris & Kasemo 1981); (iv) reactions of suprathermal species generated by the excitation and/or ionization caused by cosmic ray bombardment (Shingledecker et al. 2018; Shingledecker & Herbst 2018; Paulive, Shingledecker & Herbst 2020).

In this work, we investigated the acetaldehyde formation through a two-step mechanism based on a 'radical + ice' reaction, as done for the synthesis of formamide (CN + $H_2O_{(ice)}$: Rimola et al. 2018)) and of vinyl alcohol/ethanol (CCH + $H_2O_{(ice)}$: Perrero et al. 2022a)). Here, we propose the reaction of a methyl radical, CH_3, with a CO molecule belonging to the ice mantle of the grain, thus avoiding competitive reactions as H-abstractions, followed by a hydrogenation step:

$$CH_3 + CO \rightarrow CH_3CO \qquad (1)$$

$$CH_3CO + H \rightarrow CH_3CHO \qquad (2)$$
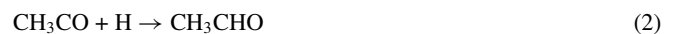
In the first step, which involves the coupling of the methyl radical CH_3 with $CO_{(ice)}$, we assume that either CH_3 is adsorbed close to the CO and diffuses to react with it (LH mechanism) or that it lands directly on the CO, reacting immediately with it (ER mechanism). The second step consists in the hydrogenation of the acetyl (CH_3CO) radical so formed, which is expected to be almost barrierless as it involves an H atom reacting with a radical, whether it diffuses on the surface (LH) or it comes from the gas-phase (ER).

This work is organized as follows: in Section 2 we report the methodology (including benchmark studies); in Section 3 we present the results and Section 4 is dedicated to their discussion and comparison with other studies. Section 5 concludes the article.

2 METHODOLOGY

2.1 Computational details

We employed CRYSTAL17 (Dovesi et al. 2018) and GAUSSIAN16 (Frisch et al. 2016) software packages, to execute periodic and molecular calculations, respectively. CRYSTAL17, at variance with other periodic codes, adopts localized Gaussian functions as basis

sets (in a similar approach to that for GAUSSIAN16), and it works with systems that range from zero to three periodic dimensions, avoiding the fake 3D replica of surface models that would arise when working with plane waves basis sets.

To reduce the computational cost of the periodic simulations, all the structures were optimized using the approximated HF-3c method followed by a single point energy calculation at the density functional theory (DFT) level, hereafter referred to as DFT//HF-3c. To check the accuracy of this scheme, we performed a benchmark study, which splits in two phases: (i) we compared the performance of DFT//HF-3c (CRYSTAL17) versus CCSD(T)//DFT in the gas-phase (GAUSSIAN16) to select the best-performing DFT functional, and (ii) we applied the ONIOM2 correction (Dapprich et al. 1999) with the extrapolation scheme of Okoshi, Atsumi & Nakai (2015) in order to compare DFT//HF-3c against ONIOM2//DFT on the surface.

The HF-3c method was used in the most time-consuming periodic calculations, namely, geometry optimizations and frequency calculations (Sure & Grimme 2013). HF-3c is based on the Hartree–Fock (HF) method computed with a minimal basis set (MINIX, Tatewaki & Huzinaga 1980), in which three empirical corrections (3c) were added: the dispersion energy D3(BJ) (Grimme et al. 2010), the basis set superposition error (BSSE) correction with the geometrical counterpoise (Kruse & Grimme 2012), and the short-range bond correction to fix overestimated covalent bond lengths for electronegative elements (Grimme, Ehrlich & Goerigk 2011; Brandenburg et al. 2013). Subsequently, the energies were refined with single point calculations on to the HF-3c optimized structures at the desired DFT level of theory, following an approach that provided accurate results in several cases, from molecular crystals (Cutini et al. 2016), polypeptides (Cutini, Corno & Ugliengo 2017), pure-silica zeolites (Cutini, Civalleri & Ugliengo 2019) to the computation of binding energies on crystalline and amorphous pure water ice (Ferrero et al. 2020; Perrero et al. 2022b).

In the periodic calculations, all the stationary points of a potential energy surfaces (PES) were characterized by the calculation of the harmonic frequencies at Γ point as minima (reactants, products) or first-order saddle points (transition states). Each Hessian matrix element was computed numerically by means of a three-point formula based on two displacements of 0.003 Å from the minimum along each Cartesian coordinate. The zero-point energy correction was computed with the standard rigid rotor/harmonic oscillator formalism (McQuarrie 1975). Since the systems are open-shell in nature, calculations were performed within the unrestricted formalism. The threshold parameters for the evaluation of the Coulomb and exchange bi-electronic integrals were set equal to 10^{-7}, 10^{-7}, 10^{-7}, 10^{-7}, and 10^{-25}. The sampling of the reciprocal space was conducted with a Pack–Monkhorst mesh (Pack & Monkhorst 1977), with a shrinking factor of 2, which generates 4k points in the first Brillouin zone.

2.2 H₂O:CO ice surface models

The H₂O:CO surfaces employed in this study were obtained from a bulk model of the pure H₂O crystalline P-ice (Casassa, Ugliengo & Pisani 1997), in which one every four water molecules was replaced by CO (Fig. 1). Three surfaces were cut along the planes (001), (010), (100) (see Fig. 2) and then fully relaxed at HF-3c level of theory, optimizing both cell parameters and atomic positions, which led to a heavy reorganization of each structure. Although we imposed a lattice to the system through periodic boundary conditions, we modelled large unit cells of H₂O:CO dirty ice (within P1 space symmetry) whose geometry relaxation resulted in an amorphous-like surface model. The cell parameters, the dipole, and the number of atoms
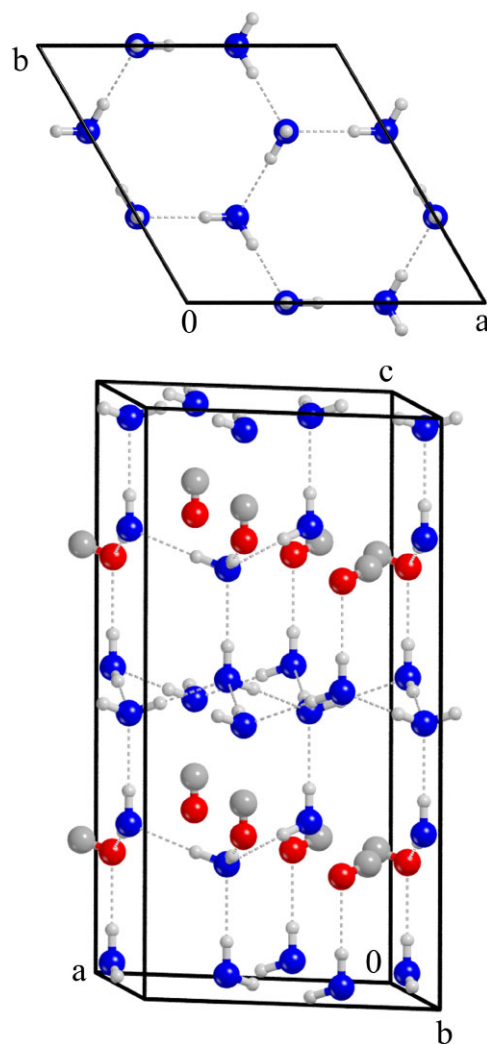

Figure 1. Top and lateral view of the dirty ice bulk model where one every four water molecules was replaced by CO. Colour code: H, white; C, grey; O atoms belonging to water, blue; O atoms belonging to the CO, red.

of each structure can be found in Table 1. The (001) surface has the smallest number of atoms (192) and the smallest dipole moment across the z-axis (−0.87 D at BHLYP-D3(BJ) level of theory). The H₂O and the CO molecules broke the symmetric structure of the bulk, creating clathrate-like cages in which CO molecules are surrounded by a network of water molecules engaged in hydrogen bonds (H-bonds). The outer layers of each surface are characterized by the presence of faintly interacting CO molecules that, depending on the coverage percentage, form a relatively complete monolayer of CO. Mixed ice models with a similar behaviour were reported in the theoretical work of Zamirri et al. (2018), in which CO adsorption, entrapment, and mixture within H₂O ices was studied. There, it emerged that dispersive and quadrupolar forces have a prominent role in determining the structural features of these ice mixtures, and are responsible for the hydrophobic behaviour of CO. Indeed, when CO is entrapped in the ice structure, it causes large rearrangements of the network of hydrogen bonds, while when it is adsorbed on the top of the surfaces, it forms ordered layers. This gives rise to sections of the surface characterized by different electrostatic potential surfaces depending on the local arrangement of the carbon monoxide molecules.
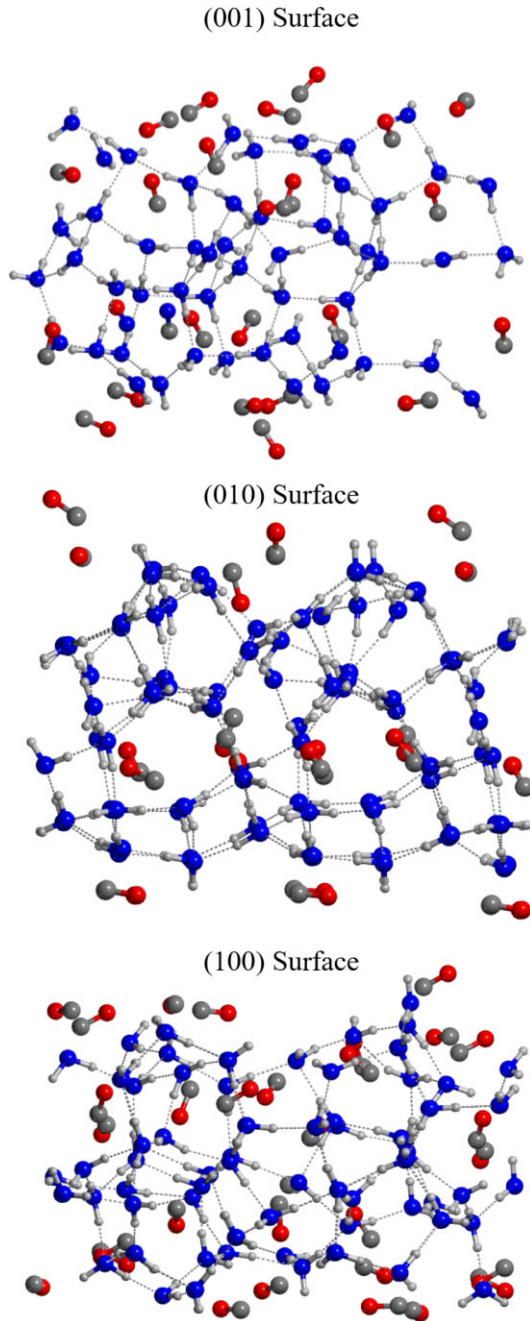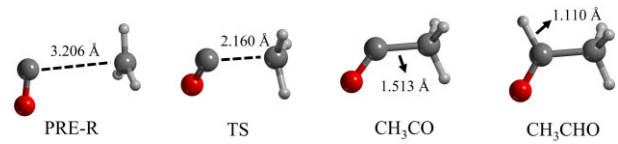
Figure 3. Stationary points of Reactions 1 and 2, computed at BHLYP-D3(BJ)/6-311G(d,p)//HF-3c level of theory. Distances are in Å.

In our model, the quantity of CO is not sufficient to give rise to a complete monolayer of CO, but the bottom face of (010) surface shows a neat arrangement of CO molecules. We notice very few cases in which CO molecules are engaged in short H-bonds with water molecules (<2.4 Å). This is because the water molecules tend to form an H-bond network between them and minimize the number of dangling H atoms pointing towards CO. Moreover, the majority of H-bond interactions take place through the O-end of the CO molecule and not through the C-end.

This phenomenon is probably driven by the small energy difference between the two interactions at HF-3c level of theory, for which the H-bond through C atom is favoured over the H-bond through the O atom by only 0.3 kJ mol^{-1} (see Fig. B1). The C···H interaction is also longer (2.390 Å) than the O···H one (2.212 Å), although the results are comparable with those given by B3LYP-D3(BJ)/6-311G(d,p).

3 RESULTS

3.1 Preliminary benchmark studies

3.1.1 Gas-phase benchmark calculations

In order to select the most appropriate DFT level of theory with which executing the periodic simulations, we first performed a benchmark analysis of the reactions 1 and 2 in the gas-phase (namely, in the absence of the whole icy surfaces). For the sake of reliability of the benchmark study adopting these gas-phase reactions, geometry optimizations were performed at HF-3c level in CRYSTAL17, while the subsequent single point energies were computed with six different DFT methods, which were corrected with the Grimme's D3 or, when available, the D3(BJ) terms (Grimme et al. 2010, 2011) to account for dispersion interactions. Thus, the employed methods are BHLYP-D3(BJ) (Lee, Yang & Parr 1988; Becke 1993a), B3LYP-D3(BJ) (Becke 1988, 1993b; Lee et al. 1988), M062X-D3 (Zhao & Truhlar 2008), M052X-D3 (Zhao, Schultz & Truhlar 2006), MPWB1K-D3(BJ) (Zhao & Truhlar 2004), and ωB97X-D3 (Chai & Head-Gordon 2008). They were used in conjunction with the Pople-based 6–311G(d,p) basis set. Diffuse functions were neglected because their small exponents can cause high linear dependencies in the wavefunction of the periodic systems we aim to work with (Klahn & Bingel 1977; VandeVondele & Hutter 2007; Peintinger, Oliveira & Bredow 2013; Vilela Oliveira et al. 2019).

The DFT//HF-3c results were compared with those obtained by performing optimizations at the same DFT/6-311G(d,p) levels, followed by single point energy calculations at single and double electronic excitation coupled-cluster method with an added perturbative description of triple excitations (CCSD(T)) combined with Dunning's aug-cc-pVTZ basis set in GAUSSIAN16 (Raghavachari et al. 1989). The reaction path is represented in Fig. 3. Reaction 1 presents a barrier due to being the coupling of the radical CH$_3$ with the closed-shell CO. Reaction 2 is a radical–radical coupling and therefore is barrierless in the gas-phase.

Figure 2. Structures of the (001), (010), and (100) ice surfaces, optimized at the HF-3c level of theory. Colour code: H, white; C, grey; O atoms belonging to water, blue; O atoms belonging to the CO, red.

Table 1. Cell parameters (a and b in Å, and γ in deg) of the three ice surfaces optimized at HF-3c level. Dipole moment (μ, in Debye) across the non-periodic z-axis of the surfaces calculated at HF-3c and BHLYP-D3(BJ) (DFT) level of theory. The number of water and carbon monoxide molecules of each surface per unit cell (H$_2$O:CO) is also reported.

Surfaces	a	b	γ	μ(HF-3c)	μ(DFT)	H$_2$O:CO
(100)	14.718	12.718	101.294	-1.78	-1.72	56:24
(010)	14.289	12.478	107.261	3.13	3.10	64:16
(001)	12.776	14.604	128.338	-1.52	-0.87	48:24

The results of this benchmark study for the gas-phase reaction models are shown in Table 2. The different CCSD(T)//DFT calculations return comparable energy values, meaning that results are almost unaffected by the small differences in the optimized geometries obtained with the different DFT methods. Thus, we only report here the results computed at CCSD(T)//BHLYP-D3(BJ), which can be taken as reference values. The error percentages on the energy barriers are high when comparing the DFT//HF-3c results with the CCSD(T)//BHLYP-D3(BJ) ones. To have deeper insights into that, we have analysed the resulting optimized structures with each method. Table 3 reports the pivotal bond lengths of each species, where one can observe that HF-3c does not reproduce well the structures for the pre-reactant (PRE-R) and the transition state (TS) structures compared with the DFT methods. In the PRE-R and in the TS, the C−C length at HF-3c versus any DFT level shows differences going from 0.1 to 0.3 Å and, indeed, have a decisive impact on the energies that are computed afterwards at single point DFT.

Energetic results indicate that B3LYP-D3(BJ) is the least suitable functional (99.3 per cent error on the potential energy barrier for Reaction 1), while BHLYP-D3(BJ) is the best one (20.6 per cent error though, corresponding to an absolute error of -4.6 kJ mol^{-1}). The BHLYP-D3(BJ) method also gives the smallest error percentage in the reaction energies for the formation of the CH_3CO radical. On the other hand, every functional describes well the reaction of CH_3CO with H.

3.1.2 Grain-surface benchmark calculations

Based on the error percentage on the energy of the gas-phase TS, we chose BHLYP-D3(BJ) to compute the reactions on the surface. However, although BHLYP-D3(BJ)//HF-3c performs globally well compared with CCSD(T)//BHLYP-D3(BJ), one has to pay special care when modelling the transition state of Reaction 1, which is the pivotal step to determine whether the reaction is feasible or not in the ISM. As probably the same discrepancies can affect the periodic calculations, we also benchmarked them to assess the quality of the employed methods. Indeed, it is clear that we need to improve the quality of our data directly on the periodic surface, where the interaction between the reactants and the ice could change again the geometrical features of the interaction between CH_3 and CO, and therefore draw more discrepancies between HF-3c, BHLYP-D3(BJ) and CCSD(T) results.

A possible solution to this problem should be performing ONIOM2 calculations (Dapprich et al. 1999) combining BHLYP-D3(BJ) with CCSD(T), as low and high energy levels. This methodology has been previously applied to the computation of binding energies (Ferrero et al. 2020; Perrero et al. 2022b). However, this would require obtaining optimized structures at BHLYP-D3(BJ) of the full periodic systems, which in our case is not feasible due to the high number of atoms present in the unit cells. Instead, we selected three test model cases for simulating the acetaldehyde formation and computing the energies applying the ONIOM2 refinement, in order to compare the performance of BHLYP-D3(BJ)//HF-3c against the ONIOM2-corrected values on the reaction barrier.

The test cases are based on two pure H_2O crystalline periodic ice models, in which one water molecule is replaced by a CO, and a molecular cluster of pure CO ice. They are shown in Fig. A1 and are represented by the 2x1 supercell of the (010) P-ice surface in which (i) a water molecule exposing a dangling oxygen atom (H_2O Ice (a)) and (ii) a water molecule exposing a dangling hydrogen atom (H_2O Ice (b)) were substituted

Table 2. Relative energies (in kJ mol^{-1}) of the stationary points of the gas-phase reactions 1 and 2 for all the DFT/6-311G(d,p) methods (computed with GAUSSIAN16). R stands for isolated reactants, PRE-R for pre-reactant complex, TS for transition state, and P for product. The data are not ZPE-corrected.

Reaction	Step	A/H†	B/H†	C/H†	D/H†	E/H†	F/H†	CCSD(T)//A†
R1: CO + CH$_3$ → CH$_3$CO	R	0.03	−0.03	4.84	6.58	1.32	1.35	2.03
	PRE-R	0.0	0.0	0.0	0.0	0.0	0	0.0
	TS	17.9	0.2	9.4	15.6	4.8	3.5	22.5
	P	−54.3	−66.4	−58.0	−51.1	−74.9	−71.6	−56.1
	err% TS R1	20.6 per cent	99.3 per cent	58.4 per cent	30.9 per cent	78.6 per cent	84.3 per cent	
	err% P R1	3.1 per cent	18.5 per cent	3.4 per cent	8.9 per cent	33.5 per cent	27.7 per cent	
	mean err% R1	11.9 per cent	58.9 per cent	30.9 per cent	19.9 per cent	56.1 per cent	56.0 per cent	
R2: CH$_3$CO + H → CH$_3$CHO	R	0.0	0.0	0.0	0.0	0.0	0.0	0.0
	P	−390.7	−388.0	−394.8	−396.8	−383.0	−402.6	−396.1
	err % P R2	1.4 per cent	2.0 per cent	0.3 per cent	0.2 per cent	3.3 per cent	1.6 per cent	

Note. † A=BHLYP-D3(BJ), B = B3LYP-D3(BJ), C = M052X-D3(BJ), D = M062X-D3, E = MPWB1K-D3(BJ), F = ωB97X-D3, H = HF-3c (computed with CRYSTAL17) and the CCSD(T)/aug-cc-pVTZ method

Table 3. Distances (in Å) of selected bonds in the structures of the pre-reactants (PRE-R), transition state (TS), and products (CH_3CO and CH_3CHO) of the gas-phase reaction models 1 and 2 computed at different theory levels.

Structure	BHLYP-D3(BJ)	B3LYP-D3(BJ)	M052X-D3	M062X-D3	MPWB1K-D3(BJ)	ωB97X-D3	HF-3c
CO	1.114	1.127	1.120	1.121	1.116	1.125	1.135
C—C (PRE-R)	3.369	3.190	3.211	3.206	3.431	3.294	3.154
C—C (TS)	2.146	2.238	2.171	2.147	2.243	2.209	2.015
C—C (CH_3CO)	1.505	1.515	1.513	1.517	1.498	1.513	1.552
C—O (CH_3CO)	1.166	1.180	1.174	1.173	1.167	1.177	1.187
C—H (CH_3CHO)	1.513	1.114	1.106	1.110	1.105	1.113	1.107
C—O (CH_3CHO)	1.177	1.204	1.200	1.199	1.191	1.200	1.208

Table 4. Potential energy barrier (in kJ mol^{-1}) of Reaction 1 computed on the three test cases for the grain-surface benchmark. DFT stands for BHLYP-D3(BJ)/6-311G(d,p).

Structure	*real*		*model*		*final*
	DFT//HF-3c	DFT//DFT	DFT	CBS	ONIOM2
H_2O Ice (a)	27.0	49.5	13.8	19.6	55.2
H_2O Ice (b)	15.1	40.1	9.0	2.3	33.3
CO Ice	11.3	15.0	18.0	20.4	17.4

by a CO molecule, and (iii) a cluster model made of 20 CO molecules.

Each system was divided in two parts (*model* and *real* systems), described by two different levels of theory (*high* and *low*). The *model* system (represented by the CH_3 and the CO) was described by the *high* level of theory, CCSD(T). The *real* system (that is, the whole system) was described by the *low* level of theory, BHLYP-D3(BJ). In this ONIOM correction, CCSD(T) was used in combination with the Dunning's aug-cc-pVNZ (with N = D,T) basis sets (Dunning 1989) and, with these data, the OAN(C) extrapolation scheme to the complete basis set (CBS) limit was applied (Okoshi et al. 2015).

The ONIOM2-corrected energy barrier (ΔE_{TS}) was computed as

$$\Delta E_{TS(ONIOM2)} = \Delta E_{TS}(low, real) +$$
$$\Delta E_{TS}(high, model) - \Delta E_{TS}(low, model), \quad (3)$$

where the $\Delta E_{corr} = \Delta E_{TS}(high,model) - \Delta E_{TS}(low,model)$ represents the correction term to the energy of the *real* system.

In this work, for the calculation of the ONIOM2-corrected barriers, ΔE_{ONIOM2}, equation (3) can be rewritten as

$$\Delta E_{TS(ONIOM2)} = \Delta E_{TS}(DFT; all) +$$
$$\Delta E_{TS}(CCSD(T)/CBS; fragm) - \Delta E_{TS}(DFT; fragm), \quad (4)$$

where ΔE_{TS}(DFT; *all*) is the activation barrier computed at DFT//DFT. The ΔE_{TS} of the model system (CH_3 + CO; *fragm*) is computed through single point energy calculations at CCSD(T)/aug-cc-pVNZ with n = D,T and extrapolated to the CBS limit due to the OAN(C) equation.

$$E_{CBS}^{OAN(C)} = \frac{3^3 E(T) - s^3 E(D)}{3^3 - s^3} \quad (5)$$

In this equation, s = 2.091 based on the choice of method and basis set, E(T) is the energy calculated with the aug-cc-pVTZ basis set, and E(D) corresponds to that computed with the aug-cc-pVDZ basis set.

We performed Reaction 1 on the three test models, both at BHLYP-D3(BJ)//HF-3c level of theory and at the ONIOM2 scheme, chosen as reference. Data are available in Table 4.
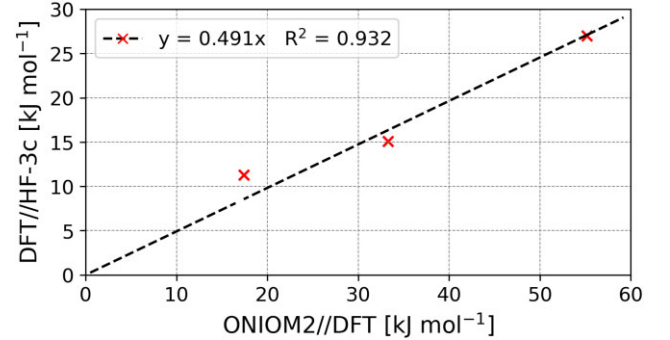
Figure 4. Plot of the DFT//HF-3c against ONIOM2//DFT potential energy barriers of Reaction 1 performed on the three test models (the CO molecular cluster and the two crystalline periodic H_2O models with a CO substitution).

In the plot of Fig. 4, we compare the ONIOM2//DFT results against the DFT//HF-3c ones. The regression line (DFT//HF-3c = 0.491·ONIOM2//DFT, R^2 = 0.932) shows that the method of choice for the periodic calculations, DFT//HF-3c, underestimates the reaction barrier, as already emerging from the gas-phase benchmark study.

Since we have very few cases, we do not aim to adopt the slope as a correction factor. On the other hand, computing the reactions on the dirty ice surface models at full BHLYP-D3(BJ) level is almost unpractical. This benchmark study, however, allows to figure out the error bar associated with the present periodic calculations.

3.2 Grain-surface reactions adopting an LH mechanism

Once we have checked and chosen a reasonably suitable methodology to calculate Reactions 1 and 2, we simulated them on the dirty H_2O:CO icy surface models.

To this end, we first adsorbed the CH_3 on the ice models by manually placing the radical in positions characterized by different local environments. Only the atomic positions were relaxed, while the cell parameters were kept frozen, to be consistent during the successive steps of the reaction and avoid structural deformations of the ice surface models. To calculate the binding energy (BE) of CH_3 on the mixed H_2O:CO surfaces, we followed the same computational scheme as in Ferrero et al. (2020) and Perrero et al. (2022b), that is, by correcting the adsorption energy $\Delta E_{ads} = E_{complex} - E_{ice} - E_{CH_3}$ for the BSSE (which generates from using a finite basis set) through the counterpoise method by Boys & Bernardi (1970).

$$BE = -\Delta E_{ads} + BSSE \quad (6)$$

For each case we computed the deformation energies of the surface and of the radical to verify that heavy structural rearrangements were not affecting our models during the geometry optimizations. We also

computed the BE(0) at 0 K, by correcting the BE for the ΔZPE as in equation (7).

$$BE(0) = BE - \Delta ZPE \qquad (7)$$

To identify the transition states, we adopted the distinguished reaction coordinate (DRC) procedure by performing a scan calculation along the C—C length. The maximum energy structure of the DRC pseudo-PES was used to localize and optimize the actual TS structure (as implemented in the CRYSTAL code, Rimola et al. 2010). In the DRC process, we avoided using internal redundant coordinates. Instead, we selected a mixed coordinate system made up of a set of selected valence internal parameters (bond lengths, angles, and dihedrals) plus the full set of symmetry adapted fractional displacements and elastic distortions (evoked by the keyword INTLMIXED in CRYSTAL17). This represents an advantage both in reducing the number of valence internal parameters that are automatically generated for the system and in solving the quasi-linear dependencies that arise in systems with a lack of connectivity, which are reflected in a very high condition number of the Wilson B-Matrix. The latter condition usually makes the optimization either to fail or to exhibit an erratic behaviour (Dovesi et al. 2018).

To simulate Reaction 2, we selected one newly formed CH_3CO/ice complex, and we manually placed the hydrogen atom to simulate its adsorption. We first set up five starting geometries and optimized the structures as open-shell triplets (the two unpaired electrons with the same sign), which were then optimized as open-shell singlets (the two unpaired electrons with opposite signs). When the orientation of H was in favour of the formation of the C—H bond, but no acetaldehyde was obtained spontaneously, we performed DRC calculations to characterize the PES of the process.

3.2.1 Adsorption of methyl radical on the dirty ices

For each surface, CH_3 was adsorbed in four different positions (two on the top-face and two on the bottom-face) to sample different binding sites. The adsorption structures at the (100) surface are shown in Fig. 5. Table 5 summarizes the computed BEs and their contribution, along with the adsorption enthalpy BE(0). The same Table 5 presents the nomenclature adopted for each binding site.

The methyl radical possesses an unpaired electron localized on the carbon atom, and its electrostatic potential surface is neutral
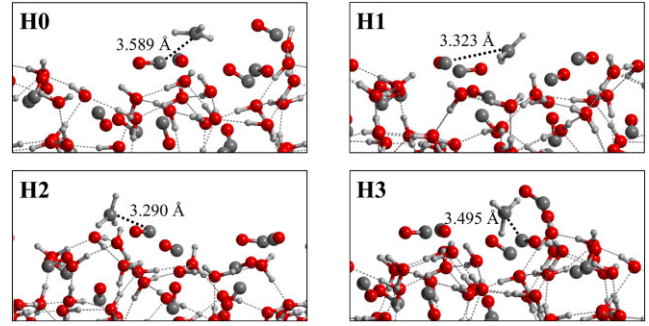

Figure 5. Structures of the CH_3 adsorption complexes on the (100) surface, optimized at HF-3c level. Distances are in Å.

almost everywhere. Therefore, this species will not form strong electrostatic interactions with the surface, especially with the polar water molecules. Thus, dispersion interactions are the key to explain the behaviour of the methyl on to the surface. The BSSE can be as large as 50 per cent of the BE, due to the fact that the 6–311G(d,p) basis set has a rather small number of functions.

The BSSE-non-corrected adsorption energies vary between −13 and −40.3 kJ mol^{-1}. Considering the BSSE, the resulting BEs range from 5.9 to 33.4 kJ mol^{-1}. In nine out of the 12 characterized binding sites, the BEs are between 6 and 14 kJ mol^{-1}, while in two cases a value of 18.5 kJ mol^{-1} is found. These values are similar to those obtained by Ferrero et al. (2020), where the BE computed on the crystalline water ice is 18.2 kJ mol^{-1}, and on the amorphous water span the 9.2 to 13.8 kJ mol^{-1} range, indicating a similar interaction of methyl radical with the two ice models. However, in the case of the binding site referred to as L3, the BE overcomes 30 kJ mol^{-1}. This is the only adsorption complex in which the interaction would be attractive even if we were not accounting for the dispersion. Indeed, while in all other cases the interaction would be repulsive, here the hydrogen atoms of the CH_3 are sufficiently close to the oxygen atoms of both CO and H_2O, therefore determining an advantageous electrostatic interaction of 8.8 kJ mol^{-1}. The ZPE correction is in the range 4–5 kJ mol^{-1} in all the cases, as we would expect from the limited rearrangement of both the surface and the radical upon adsorption.

Table 5. Binding energy (BE) values (in kJ mol^{-1}) of CH_3 on different surface sites of the dirty H_2O:CO ice model. The contributions from the pure potential energy values (ΔE_{ads}), the BSSE corrections ($\Delta BSSE$), the dispersive (Disp) and the non-dispersive (No Disp) terms of the BE, the zero-point energy corrections (ΔZPE), and the resulting adsorption enthalpy (BE(0)) are shown.

Surface	Binding site	ΔE_{ads}	$\Delta BSSE$	BE	Disp	No disp	ΔZPE	BE(0)
(100)	H0	−15.2	−5.9	9.3	15.0	−5.7	4.0	5.3
	H1	−18.8	−8.9	9.8	17.8	−8.0	4.7	5.1
	H2	−17.4	−6.8	10.7	13.3	−2.6	3.7	7.0
	H3	−22.2	−10.8	11.3	20.2	−8.8	4.7	6.7
(010)	K0	−27.3	−13.4	14.0	19.8	−5.8	4.5	9.5
	K1	−14.5	−6.2	8.3	12.9	−4.6	4.4	3.9
	K2	−31.8	−13.4	18.4	18.8	−0.4	4.7	13.7
	K3	−29.4	−11.0	18.5	16.9	1.5	4.3	14.1
(001)	L0	−13.8	−7.3	6.5	6.7	−0.2	5.5	1.0
	L1	−13.0	−7.1	5.9	27.9	−22.0	6.6	−0.7
	L2	−18.9	−7.6	11.3	14.7	−3.3	3.9	7.4
	L3	−40.3	−6.9	33.4	24.5	8.8	4.3	29.1

Table 6. ZPE-corrected potential energy barriers ($\Delta H(0)_{TS}$, in kJ mol^{-1}) for the formation of acetyl on different binding sites of each surface. The internal potential energy values (ΔE_{TS}) and the zero-point energy corrections (ΔZPE_{TS}) are displayed.

Surface	Binding site	ΔE_{TS}	ΔZPE_{TS}	$\Delta H(0)_{TS}$
(100)	H1	11.7	10.7	22.4
	H2	13.4	11.3	24.7
	H3	5.8	11.0	16.8
(010)	K1	11.6	10.3	21.9
	K2	23.7	10.0	33.7
	K3	36.8	10.1	46.9
(001)	L1	10.8	10.8	21.6
	L2	14.5	12.3	26.8
	L3	14.4	11.9	26.5
Gas-phase	-	17.9	10.8	28.7

3.2.2 Acetyl radical formation

We modelled the formation of acetyl on a selected number of structures (see Fig. C1 for an example). For each surface, we chose the three adsorption complexes characterized by the largest differences in the chemical environment of CH$_3$. The purpose of this choice is to probe the effect of the chemical environment on the potential energy barrier of the reaction. According to the LH mechanism, the CH$_3$ diffuses towards the closest CO on the surface to form the chemical bond. In all the nine cases analysed (see Table 6), a potential energy barrier has to be overcome in order to form the acetyl radical. The average barrier is around 10–15 kJ mol^{-1}, with some exceptions. On the (100) surface, the complex **H3** has a barrier of only 5.8 kJ mol^{-1}. We notice that in this case, in the scan calculation, it is the CO that approaches the CH$_3$ and not vice versa, as we observed in the other simulations. We suppose that the particular geometry of this surface allows an easy diffusion of the CO, turning into a low potential energy barrier. On the other hand, on the (010) surface, we found two unfavourable mechanisms, **K2** and **K3**, presenting energy barriers up to 36.8 kJ mol^{-1}. In **K2**, an H-bond between the carbon of the CO and a water molecule of the surface needs to break to make CO available for the reaction with CH$_3$. In **K3**, the large distance (3.9 Å) between the reactants is the responsible of the high barrier.

When adding the ZPE contributions, according to the equation $\Delta H_{TS} = \Delta E_{TS} + \Delta ZPE$, each barrier increases by about 11 kJ mol^{-1}. For the gas-phase reaction, we found barriers of $\Delta E_{TS} = 17.9$ kJ mol^{-1} and $\Delta H_{TS} = 28.7$ kJ mol^{-1}, meaning a $\Delta ZPE_{TS} = 10.8$ kJ mol^{-1}, very close to that obtained on the surface. If we focus solely on the energy barrier, in seven cases out of nine the barriers of the surface reactions are lower than the gas-phase one. However, the grain-surface benchmark calculations warn us that these barriers are underestimated and therefore it is highly probable that only the grain-surface **H3** case is slightly more favourable than the gas-phase reaction.

3.2.3 Acetaldehyde formation

Among the different acetyl products obtained, we selected the **H1** case to model Reaction 2. The reason for this choice is that, in this structure, the acetyl is bound to a water molecule through an H-bond involving the oxygen of the carbonyl group, which means the carbon atom of interest is not hindered because it is pointing towards the gas-phase (it is not facing the inner side of the surface), and thus it is prone to react with a hydrogen atom diffusing on the surface (see Fig. C2).

The adsorption of atomic hydrogen followed by the optimization of the CH$_3$CO + H complex in an open-shell triplet spin state resulted, as expected, in no reaction. However, a change of the electronic spin state to an open-shell singlet brought to the spontaneous formation of acetaldehyde in two (out of five) complexes without harming the H-bond interaction between the carbonyl moiety and the H$_2$O$_{(ice)}$. We noticed that if the H atom is at a maximum distance of 3.5 Å from the CO moiety and it is correctly oriented (meaning that it approaches the CO from the less hindered side), the radical coupling is barrierless.

In the other cases, either the H atom is hindered by the methyl moiety, or it has to overcome a small diffusion barrier to get close enough to the reactive centre. With the methodology chosen for the optimization, we notice that a very small diffusion barrier, of about 1 kJ mol^{-1}, is limiting the free diffusion of the hydrogen on the surface, as the gradient in the optimization process falls to zero and a minimum is found.

3.3 Grain-surface reactions adopting an ER mechanism

In the ER mechanism, the CH$_3$ gas-phase species directly reacts with a surface CO icy component. To simulate this, we generated, with a Python script, several geometries in which the distance between the approaching CH$_3$ from the gas-phase and the reactive CO of the surface progressively decreases. We ran the optimization of these structures without relaxing the geometry of the surface to avoid its thermalization during the approach of the CH$_3$. Only after the product forms, the entire system was relaxed. Therefore, we provide the energy profiles for Reactions 1 and 2 without characterizing the actual transition states but only giving an estimate. This is because, due to the geometrical constraints applied to the surface, we would obtain high-order stationary points with imaginary frequencies associated with the motion of the frozen atoms of the surface. For the same reason, we also do not provide the ZPE-corrected profiles for these processes. We simulated both steps of the reaction assuming an ER mechanism. We chose the (100) surface as the reactive one, focusing on the **H1** binding site. We did so in order to compare LH and ER mechanisms for steps 1 and 2, but also because the CO involved in the C—C bond formation is exposing the C-end towards the gas-phase, therefore being available for this type of reactivity. The energy profile of CH$_3$ + CO is plotted in Fig. 6. Both the profile computed at HF-3c level and the one refined at BHLYP-D3(BJ) level are shown. One can clearly see the disagreement between the two methodologies in terms of energetics. The BHLYP-D3(BJ) profile shows that below 5 Å of distance there is an attractive interaction between the methyl radical and the CO. The presence of a van der Waals complex well in the energy profile appears at a distance of 3.3 Å. When getting close to 2 Å, we find the maximum energy point, whose value is about 8.5 kJ mol^{-1} compared with the energy at infinite distance. The ΔE between the minimum and maximum energy point is 16 kJ mol^{-1}, which is compatible with the barrier computed for the LH mechanism. According to these results, with both the formation of such complex and the presence of a barrier, the reaction will hardly yield acetyl.

On the other hand, considering that acetyl is already on the surface and a hydrogen atom approaches from the gas-phase, two situations can take place (see Fig. 7). If the overall spin of the system is a triplet, no coupling takes place and the energy of the system becomes highly repulsive as the distance between the two reactants increase. In contrast, if the system is in a singlet open-shell electronic state, the formation of the C—H bond occurs spontaneously. We also simulated the competitive reaction, in which H falls on to the surface and
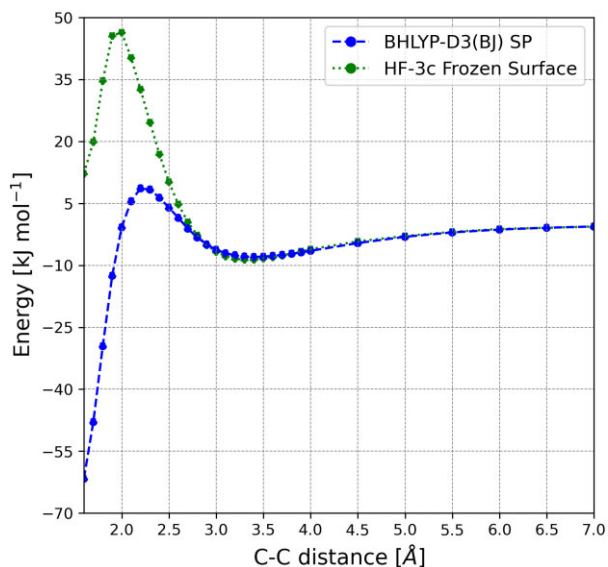
Figure 6. Eley–Rideal reaction profile of CH$_3$ + CO. Energy is given in kJ mol^{-1}, C—C distance in Å. The reaction is computed keeping the surface frozen at HF-3c level of theory (green). We also provide the single point energy computed at BHLYP-D3(BJ)/6-311G(d,p) level of theory (blue) on HF-3c geometries.
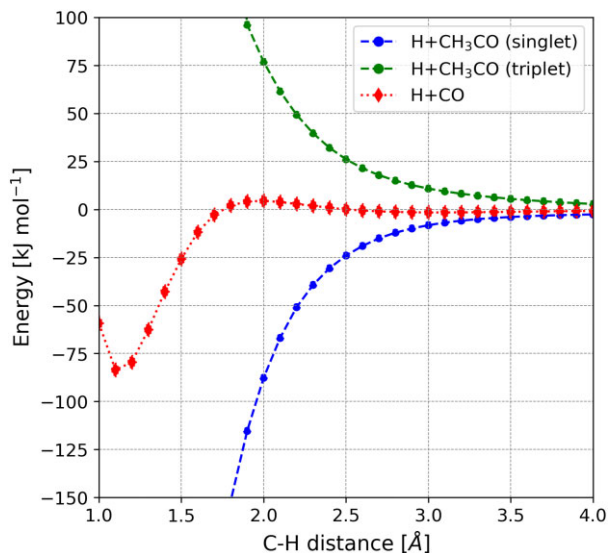

Figure 7. Eley–Rideal reaction profile of H + CH$_3$CO and its competitive reaction H + CO at BHLYP-D3(BJ)/6-311G(d,p) level of theory. Energy is given in kJ mol^{-1}, C—H distance in Å. H + CO presents a small barrier (red), H + CH$_3$CO in the triplet spin state (green) becomes repulsive, while in the singlet spin state (blue) yields the product barrierlessly.

reacts with an adjacent surface CO molecule (considering an overall triplet spin state) forming the HCO radical with a small barrier of 4.5 kJ mol^{-1}. Thus, in case of an H atom approaching the surface, the formation of acetaldehyde via H addition to acetyl is the most probable reaction.

4 DISCUSSION AND ASTROPHYSICAL IMPLICATIONS

In this work, we simulated the formation of acetaldehyde on H$_2$O:CO dirty ice surfaces models through the reaction of a methyl radical with a CO belonging to the ice surface, in which, subsequently, the newly formed acetyl radical gets hydrogenated to yield acetaldehyde. We performed these two-step process on the basis of both LH and ER surface mechanisms.

Due to this 'radical + ice' reaction mechanism, step 1 has no competitive reactions, at variance with the prevailing radical–radical coupling mechanism (Enrique-Romero et al. (2022)). Indeed, in our case, CH$_3$ cannot extract a hydrogen atom from water to yield CH$_4$, neither we consider such a high abundance for CH$_3$ to be able to form ethane (CH$_3$CH$_3$). As far as Reaction 2 is concerned, there may be a competitive channel, i.e. H + CO → HCO, known to have a barrier of ~5 kJ mol^{-1} and to occur through tunnelling (e.g. Rimola et al. 2014; Pantaleone et al. 2020). In our simulations, we also observe the presence of a barrier. Even though we modelled the process through an ER mechanism and we did not isolate the exact transition state of this reaction, the energy profile reaches its maximum of energy at 4.5 kJ mol^{-1}. In contrast, the formation of acetaldehyde is barrierless and therefore favoured.

The benchmark that we performed for the acetyl formation reaction on the icy surfaces stresses that the BHLYP-D3(BJ)//HF-3c computational scheme seems to underestimate the potential energy barrier of the process. Thus, a direct comparison with the gas-phase reaction (computed at full DFT level) is therefore not possible. However, if we roughly assume that the computed $\Delta E(0)_{TS}$ values on the surfaces have to be doubled to be fairly compared with the gas-phase ones (as emerged from the benchmark study), it turns out that the grain-surface reactions are less favourable than the gas-phase ones in the majority of the cases, namely, just one case out of nine is characterized by a $\Delta H(0)_{TS}$ lower than the 28.7 kJ mol^{-1} found for the gas-phase reaction. However, even in the most favourable case, the barrier is still high so that Reaction 1 is unlikely to take place in the cold molecular clouds. Additionally, in environments where the temperature can be higher (namely, with more thermal energy available to overcome the barrier), the sublimation of CO and CH$_3$ (above 20 K: e.g. Ferrero et al. 2020) will prevent the reaction from taking place.

Therefore, we can summarize the effect of the ice surface on the acetyl formation through the reaction of CH$_3$ with iced CO in two points: (i) the CO embedded in the surface is not strongly activated towards the reaction by the surrounding icy water molecules, which in fact, if possible, avoid interacting with the CO molecules by creating clathrate-like structures, as it appears during the optimization of the surfaces; and (ii) in almost all the surface reactions, the potential energy barrier is fairly larger than that in the gas-phase, meaning that there is an additional, although modest, interaction between the CH$_3$ radical and the surface that needs to be broken in order to allow the radical to approach the CO and form a C—C bond.

On the other hand, the second step (formation of acetaldehyde by H-addition to acetyl) is favoured by the presence of the ice, as the surface is well known to act as a reactant concentrator (e.g. Ioppolo, Cuppen & Linnartz 2011; Rimola et al. 2014; Fedoseev et al. 2015; Simons et al. 2020; Ferrero et al. 2023b) as well as third body (i.e. energy dissipator, hence stabilizing the newly formed product) (e.g. Pantaleone et al. 2020, 2021; Molpeceres et al. 2023; Ferrero et al. 2023a) in hydrogenation of atoms and small molecules. Moreover, in the event that hydrogen is approaching the acetyl with an unfavourable orientation, due to its easy diffusion, it is able to move towards the CO moiety and yield acetaldehyde.

The ER mechanism does not bring any improvement over the LH one. For the former, to be effective, the acetyl formation should not have a barrier, this way avoiding the preliminary adsorption and forming directly the product. Ruaud et al. (2015) stress the importance of this mechanism for reactions between atomic carbon and icy components. However, in our case, both mechanisms present a barrier with similar heights, so that none of the mechanisms dominate over the other (at least from an energetic standpoint). For the hydrogenation of the acetyl radical to form acetaldehyde, both mechanisms are feasible to yield the product, although the LH one is probably favoured due to the fact that at a temperature as low as 10 K the majority of atomic hydrogen would probably be adsorbed on the surface. We have seen, moreover, that the relative orientation between H and acetyl is not a hampering factor so that probably, at 10 K, H atoms have enough mobility to jump between different adsorption sites and find the orientation that would favour the formation of acetaldehyde.

Therefore, although the $CH_3 + CO_{(ice)}$ mechanism seems not to particularly enhance the formation of acetaldehyde, this result is important to constraint the active synthetic paths that drive the formation of acetaldehyde in the ISM.

Other studies have focused on acetaldehyde grain-surface formation through radical recombination between HCO and CH_3 (e.g. Enrique-Romero et al. 2016, 2019, 2021; Lamberts et al. 2019), which already highlighted the difficulty of the synthesis of this iCOM. In Enrique-Romero et al. (2016) and Enrique-Romero et al. (2019), the reactivity between CH_3 and HCO performed on H_2O ice resulted in either formation of acetaldehyde or in $CH_4 + CO$ due to a competitive H abstraction, both reactions having small or no potential energy barriers. In a subsequent work, Enrique-Romero et al. (2021) found that the efficiency of acetaldehyde formation was overall low in comparison with that of $CH_4 + CO$. In Lamberts et al. (2019), the radical pair reactivity was investigated on CO ices by means of *ab initio* molecular dynamics. By adopting a sufficient configurational sampling (namely, different trajectories based on different initial guess structures), the authors found that the reactivity results in either no reaction, formation of CH_3CHO, or $CH_4 + CO$, the last two outcomes being barrierless, while in the first case the non-formation of a product was due to the presence of a barrier. Therefore, according to these results, acetaldehyde synthesis on icy surfaces is not a favourable path. This is in agreement with the theoretical study by Simons et al. (2020), who stated that the reaction network obtained by the hydrogenation of CO may cause the production of several iCOMs (glycolaldehyde, ethylene glycol, and to a less extent methyl formate), alongside methanol and formaldehyde, but acetaldehyde is not one of them. Likewise, the experimental study by Gutiérrez-Quintanilla et al. (2021) found that acetaldehyde is not formed by the combination of radicals created by the UV illumination of methanol ice.

An alternative way of forming acetaldehyde on the grain-surfaces discussed in the literature is via the reaction of carbon atoms with the CO molecules of the ices. Fedoseev et al. (2022) experimentally studied the reaction of C + CO co-deposited with H_2O and H at 10 K, following the theoretical study of Papakondylis & Mavridis (2019). The authors observed the formation of CCO and its hydrogenated counterpart, the ketene CH_2CO. Successive hydrogenation steps result in CH_3CHO. Likewise, Ferrero et al. (2023b) carried out a theoretical study on the formation of ketene from the reaction of C with $CO_{(ice)}$ and the potential successive reactions with radicals (e.g. OH and NH_2) that could form other iCOMs and found that only hydrogenation (via H-tunneling), eventually leading to acetaldehyde could occur, because of important energy barriers. However, as Ferrero et al. (2023b) noticed, the simultaneous presence of gaseous atomic carbon landing on the grain-surfaces and a CO-rich ice is very unlikely in the molecular ISM, except in photodissociation regions, as abundant frozen CO implies an evolved molecular cloud or pre-stellar core where atomic carbon has an extremely low abundance.

Assuming that CH_3CHO is formed on the grain-surfaces, then a thermal and/or non-thermal mechanism is needed to partially transfer it into the gas-phase, where it is observed. This is particularly problematic when considering the detection of acetaldehyde in several cold pre-stellar cores (Scibelli & Shirley 2020). The parameter establishing whether a species stays bound to the icy mantle or enriches the gas-phase is its BE. A recent computational work by Ferrero et al. (2022) highlights how the acetaldehyde BE, ranging from 3000 to 7000 K on water ice, represents an obstacle to explain its presence in the gas-phase of cold environments. The studies by Corazzi et al. (2021) and Molpeceres et al. (2022) reported a value which is close to the lower end of the distribution outlined in Ferrero et al. (2022), but it is still too large to allow desorption in cold (10 K) astronomical objects. Usually, to explain the desorption process of this and other iCOMs, non-thermal mechanisms such as photodesorption, reactive desorption, and cosmic-ray desorption are invoked (e.g. Dulieu et al. 2013; Chuang et al. 2018; Dartois et al. 2019), each of these mechanism having their drawbacks (e.g. Bertin et al. 2016; Pantaleone et al. 2020). Clearing this matter is out of the scope of this work, which aims at investigating acetaldehyde formation on icy surfaces.

In summary, all studies so far carried out, theoretical and experimental, tend to agree that acetaldehyde is unlikely to be a grain-surface product. On the contrary, several studies now seem to favour the hypothesis of acetaldehyde formed in the gas-phase. We would like to mention in particular the work by Vazart et al. (2020), who showed a very good agreement between the observed and measured abundance of acetaldehyde in hot corinos.

5 CONCLUSIONS

In this work, we studied the formation of acetaldehyde (CH_3CHO) on the grain surfaces through a two-step mechanism: (i) the reaction of a methyl (CH_3) radical with a CO molecule belonging to a periodic surface of H_2O:CO dirty ice to form acetyl (CH_3CO), and (ii) the hydrogenation of the newly formed acetyl. We characterized the process via the Langmuir–Hinshelwood and Eley–Rideal mechanisms and compared the results obtained against those simulated for the same reaction in the gas-phase. Our grain-surface benchmark on three test models stressed that the barriers computed at BHLYP-D3(BJ)//HF-3c level are fairly underestimated against CCSD(T)//BHLYP-D3(BJ).

We modelled three periodic dirty ice surfaces by cutting along the planes (001), (010), and (100) a bulk of crystalline H_2O P-ice, where one-fourth of the water molecules was substituted by CO. We obtained three amorphous-like surfaces characterized by a variable content in CO on to which we simulated several adsorption structures of CH_3, finding that dispersion interactions are crucial for the adsorption process. We computed the ZPE-corrected PES of acetyl formation in three cases for each H_2O:CO ice surface, results pointing out that in most of the cases the reaction presents high energy barriers insurmountable in the ISM. The formation of acetyl via $CH_3 + CO_{(ice)}$ on the surface is less favourable than its gas-phase counterpart in the majority of the cases.

We have elucidated that these overall unfavourable reactions are due to that (i) the CO molecule is hardly activated by the surface and the CH_3 does not present an enhanced reactivity (it does not form hemibonded systems), and (ii) the barriers for acetyl formation

depend on the local environment of the CO, that is, they are high (in most of the cases) when the distance between the reactants is large or when the CO/H$_2$O interactions have to be broken for the reaction to take place. On the other hand, the hydrogenation of acetyl is barrierless, given that the electronic spin of the system is a singlet open-shell and that the H atom is so mobile that it always finds a proper orientation towards the carbonyl group of CH$_3$CO. The outcome of the reaction, specifically its barrier, does not improve when adopting the ER mechanism against the LH one.

In summary, several previous studies have challenged the hypothesis that acetaldehyde is formed on the grain-surfaces via the combination of on-surface radicals, specifically CH$_3$ and HCO (e.g. Enrique-Romero et al. 2016, 2019, 2021; Lamberts et al. 2019; Simons et al. 2020; Gutiérrez-Quintanilla et al. 2021). Leveraging on other studies showing that some iCOMs (ethanol and formamide: Rimola et al. 2018; Perrero et al. 2022a) could be formed on the grain surfaces via reactions of radicals with molecules belonging to the ice, in this work, we investigated the reaction of the CH$_3$ radical with one CO molecule of the ice. Our computations show that also this path is unfavourable to the acetaldehyde formation, reducing the possibilities that the latter is formed on the grain surfaces. Alternatively, gas-phase reactions could be at the origin of the almost ubiquitous presence of acetaldehyde in the ISM (e.g. Vazart et al. 2020).

DATA AVAILABILITY

The data underlying this article are freely available in Zenodo at https://doi.org/10.5281/zenodo.7937759.

REFERENCES

Alexander C. M. O., Cody G. D., Kebukawa Y., Bowden R., Fogel M. L., Kilcoyne A. L. D., Nittler L. R., Herd C. D. K., 2014, Meteorit. Planet. Sci., 49, 503

Bacmann A., Taquet V., Faure A., Kahane C., Ceccarelli C., 2012, A&A, 541, L12

Balucani N., Ceccarelli C., Taquet V., 2015, MNRAS, 449, L16

Becke A. D., 1988, Phys. Rev. A, 38, 3098

Becke A. D., 1993a, J. Chem. Phys., 98, 1372

Becke A. D., 1993b, J. Chem. Phys., 98, 5648

Ben Chouikha I., Kerkeni B., Ouerfelli G., Makroni L., Nyman G., 2022, RSC Adv., 12, 18994

Bennett C. J., Osamura Y., Lebar M. D., Kaiser R. I., 2005, ApJ, 634, 698

Bergner J. B., Öberg K. I., Rajappan M., 2017, ApJ, 845, 29

Bergner J. B., Öberg K. I., Rajappan M., 2019, ApJ, 874, 115

Bertin M. et al., 2016, ApJ, 817, L12

Bianchi E. et al., 2019, MNRAS, 483, 1850

Biver N. et al., 2021, A&A, 648, A49

Blake G. A., Sutton E. C., Masson C. R., Phillips T. G., 1987, ApJ, 315, 621

Boys S., Bernardi F., 1970, Mol. Phys., 19, 553

Brandenburg J. G., Alessio M., Civalleri B., Peintinger M. F., Bredow T., Grimme S., 2013, J. Phys. Chem. A, 117, 9282

Callahan M. P., Smith K. E., Cleaves H. J., Ruzicka J., Stern J. C., Glavin D. P., House C. H., Dworkin J. P., 2011, Proc. Natl. Acad. Sci., 108, 13995

Casassa S., Ugliengo P., Pisani C., 1997, J. Chem. Phys., 106, 8030

Caselli P., Ceccarelli C., 2012, A&AR, 20, 56

Cazaux S., Tielens A. G. G. M., Ceccarelli C., Castets A., Wakelam V., Caux E., Parise B., Teyssier D., 2003, ApJ, 593, L51

Ceccarelli C. et al., 2014, in Beuther H., Klessen R. S., Dullemond C. P., Henning T., eds, Protostars and Planets VI. University of Arizona Press, Tucson, AZ, p. 859

Ceccarelli C. et al., 2017, ApJ, 850, 176

Ceccarelli C. et al., 2022, Protostars and Planets VII, (arXiv:2206.13270)

Chahine L. et al., 2022, A&A, 657, A78

Chai J.-D., Head-Gordon M., 2008, J. Chem. Phys., 128, 084106

Charnley S., 2004, Adv. Space Res., 33, 23

Charnley S. B., Tielens A. G. G. M., Millar T. J., 1992, ApJ, 399, L71

Charnley S. B., Tielens A. G. G. M., Rodgers S. D., 1997, ApJ, 482, L203

Chuang K.-J., Fedoseev G., Qasim D., Ioppolo S., van Dishoeck E. F., Linnartz H., 2018, ApJ, 853, 102

Chuang K.-J., Fedoseev G., Scirè C., Baratta G. A., Jäger C., Henning T., Linnartz H., Palumbo M. E., 2021, A&A, 650, A85

Codella C. et al., 2018, A&A, 617, A10

Corazzi M. A., Brucato J. R., Poggiali G., Podio L., Fedele D., Codella C., 2021, ApJ, 913, 128

Crovisier J., Bockelée-Morvan D., Colom P., Biver N., Despois D., Lis D. C., the Team for target-of-opportunity radio observations of comets, 2004, A&A, 418, 1141

Cutini M., Civalleri B., Corno M., Orlando R., Brandenburg J. G., Maschio L., Ugliengo P., 2016, J. Chem. Theory Comput., 12, 3340

Cutini M., Corno M., Ugliengo P., 2017, J. Chem. Theory Comput., 13, 370

Cutini M., Civalleri B., Ugliengo P., 2019, ACS Omega, 4, 1838

Dapprich S., Komáromi I., Byun K., Morokuma K., Frisch M., 1999, Comput. Theor. Chem., 461–462, 1

Dartois E., Chabot M., Id Barkach T., Rothard H., Augé B., Agnihotri A. N., Domaracka A., Boduch P., 2019, A&A, 627, A55

De Simone M. et al., 2020, A&A, 640, A75

Dovesi R. et al., 2018, WIREs Comp. Mol. Sci., 8, e1360

Drozdovskaya M. N., van Dishoeck E. F., Rubin M., Jørgensen J. K., Altwegg K., 2019, MNRAS, 490, 50

Dulieu F., Congiu E., Noble J., Baouche S., Chaabouni H., Moudens A., Minissale M., Cazaux S., 2013, Sci. Rep., 3, 1338

Dunning T. H., 1989, J. Chem. Phys., 90, 1007

Eley D., Rideal E., 1940, Nature, 146, 401

Enrique-Romero J., Rimola A., Ceccarelli C., Balucani N., 2016, MNRAS, 459, L6

Enrique-Romero J., Rimola A., Ceccarelli C., Ugliengo P., Balucani N., Skouteris D., 2019, ACS Earth Space Chem., 3, 2158

Enrique-Romero J. et al., 2020, MNRAS, 493, 2523

Enrique-Romero J., Ceccarelli C., Rimola A., Skouteris D., Balucani N., Ugliengo P., 2021, A&A, 655, A9

Enrique-Romero J., Rimola A., Ceccarelli C., Ugliengo P., Balucani N., Skouteris D., 2022, ApJS, 259, 39

Fedoseev G., Cuppen H. M., Ioppolo S., Lamberts T., Linnartz H., 2015, MNRAS, 448, 1288

Fedoseev G., Qasim D., Chuang K.-J., Ioppolo S., Lamberts T., van Dishoeck E. F., Linnartz H., 2022, ApJ, 924, 110

Ferrero S., Zamirri L., Ceccarelli C., Witzel A., Rimola A., Ugliengo P., 2020, ApJ, 904, 11

Ferrero S. et al., 2022, MNRAS, 516, 2586

Ferrero S., Pantaleone S., Ceccarelli C., Ugliengo P., Sodupe M., Rimola A., 2023a, ApJ, 944, 142

Ferrero S., Ceccarelli C., Ugliengo P., Sodupe M., Rimola A., 2023b, ApJ, 951, 150

Fourikis N., Sinclair M. W., Robinson B. J., Godfrey P. D., Brown R. D., 1974, Aust. J. Phys., 27, 425

Frisch M. J. et al., 2016, Gaussian 16 Revision C.01

Garrod R. T., Herbst E., 2006, A&A, 457, 927

Garrod R. T., Weaver S. L. W., Herbst E., 2008, ApJ, 682, 283

Gilmore W., Morris M., Johnson D. R., Lovas F. J., Zuckerman B., Turner B. E., Palmer P., 1976, ApJ, 204, 43

Gottlieb C. A., 1973, in Gordon M. A., Snyder L. E., eds, Molecules in the Galactic Environment, Harvard University, Cambridge, Massachusetts, p. 181

Grimme S., Antony J., Ehrlich S., Krieg H., 2010, J. Chem. Phys., 132, 154104

Grimme S., Ehrlich S., Goerigk L., 2011, J. Comp. Chem., 32, 1456

Gutiérrez-Quintanilla A. et al., 2021, MNRAS, 506, 3734

Harris J., Kasemo B., 1981, Surf. Sci., 105, L281

Hasegawa T. I., Herbst E., 1993, MNRAS, 263, 589

Herbst E., 2017, Int. Rev. Phys. Chem., 36, 287

Herbst E., van Dishoeck E. F., 2009, ARA&A, 47, 427

Hinshelwood C., 1930, Annu. Rep. Prog. Chem., 27, 11

Ioppolo S., Cuppen H., Linnartz H., 2011, Rend. Fis. Acc. Lincei, 22, 211

Jin M., Garrod R. T., 2020, ApJS, 249, 26

Klahn B., Bingel W. A., 1977, Int. J. Quantum Chem., 11, 943

Krasnokutski S. A., Jäger C., Henning T., 2020, ApJ, 889, 67

Kruse H., Grimme S., 2012, J. Chem. Phys., 136, 154101

Lamberts T., Markmeyer M. N., Kolb F. J., Kästner J., 2019, ACS Earth Space Chem., 3, 958

Langmuir I., 1922, Trans. Faraday Soc., 17, 621

Öberg K. I., van Dishoeck E. F., Linnartz H., Andersson S., 2010, ApJ, 718, 832

Law C. J., Zhang Q., Öberg K. I., Galván-Madrid R., Keto E., Liu H. B., Ho P. T. P., 2021, ApJ, 909, 214

Lee C., Yang W., Parr R. G., 1988, Phys. Rev. B, 37, 785

Lee C.-F., Codella C., Li Z.-Y., Liu S.-Y., 2019, ApJ, 876, 63

Lefloch B., Ceccarelli C., Codella C., Favre C., Podio L., Vastel C., Viti S., Bachiller R., 2017, MNRAS Letters, 469, L73

Ligterink N. F. W. et al., 2018, A&A, 619, A28

Martín-Doménech R., Öberg K. I., Rajappan M., 2020, ApJ, 894, 98

Matthews H. E., Friberg P., Irvine W. M., 1985, ApJ, 290, 609

McClure M. K. et al., 2023, Nat. Astron., 7, 1

McElroy D., Walsh C., Markwick A. J., Cordiner M. A., Smith K., Millar T. J., 2013, A&A, 550, A36

McQuarrie D. A., 1975, Statistical Mechanics. Harper and Row, New York

Molpeceres G., Kästner J., Herrero V. J., Peláez R. J., Maté B., 2022, A&A, 664, A169

Molpeceres G., Zaverkin V., Furuya K., Aikawa Y., Kästner J., 2023, A&A, 673, A51

Moore M. H., Hudson R. L., 1998, Icarus, 135, 518

Öberg K. I., Garrod R. T., Van Dishoeck E. F., Linnartz H., 2009, A&A, 504, 891

Okoshi M., Atsumi T., Nakai H., 2015, J. Comp. Chem., 36, 1075

Paardekooper D., Bossa J.-B., Linnartz H., 2016, A&A, 592, A67

Pack J. D., Monkhorst H. J., 1977, Phys. Rev. B, 16, 1748

Pantaleone S., Enrique-Romero J., Ceccarelli C., Ugliengo P., Balucani N., Rimola A., 2020, ApJ, 897, 56

Pantaleone S., Enrique-Romero J., Ceccarelli C., Ferrero S., Balucani N., Rimola A., Ugliengo P., 2021, ApJ, 917, 49

Papakondylis A., Mavridis A., 2019, J. Phys. Chem. A, 123, 10290

Paulive A., Shingledecker C. N., Herbst E., 2020, MNRAS, 500, 3414

Peintinger M. F., Oliveira D. V., Bredow T., 2013, J. Comp. Chem., 34, 451

Perrero J., Enrique-Romero J., Martínez-Bachs B., Ceccarelli C., Balucani N., Ugliengo P., Rimola A., 2022a, ACS Earth Space Chem., 6, 496

Perrero J., Enrique-Romero J., Ferrero S., Ceccarelli C., Podio L., Codella C., Rimola A., Ugliengo P., 2022b, ApJ, 938, 158

Raghavachari K., Trucks G. W., Pople J. A., Head-Gordon M., 1989, Chem. Phys. Lett., 157, 479

Rimola A., Zicovich-Wilson C. M., Dovesi R., Ugliengo P., 2010, J. Chem. Theory Comput., 6, 1341

Rimola A., Taquet V., Ugliengo P., Balucani N., Ceccarelli C., 2014, A&A, 572, A70

Rimola A., Skouteris D., Balucani N., Ceccarelli C., Enrique-Romero J., Taquet V., Ugliengo P., 2018, ACS Earth Space Chem., 2, 720

Rotelli L., Trigo-Rodríguez J. M., Moyano-Cambero C. E., Carota E., Botta L., di Mauro E., Saladino R., 2016, Sci. Rep., 6, 38888

Ruaud M., Loison J. C., Hickson K. M., Gratier P., Hersant F., Wakelam V., 2015, MNRAS, 447, 4004

Scibelli S., Shirley Y., 2020, ApJ, 891, 73

Shingledecker C. N., Herbst E., 2018, Phys. Chem. Chem. Phys., 20, 5359

Shingledecker C. N., Tennis J., Gal R. L., Herbst E., 2018, ApJ, 861, 20

Simons M. A. J., Lamberts T., Cuppen H. M., 2020, A&A, 634, A52

Singh K. K., Tandon P., Misra A., 2019, in Singh D. K., Das S., Materny A.eds, Advances in Spectroscopy: Molecules to Materials. Springer Singapore, Singapore, p. 415

Skouteris D., Balucani N., Ceccarelli C., Vazart F., Puzzarini C., Barone V., Codella C., Lefloch B., 2018, ApJ, 854, 135

Sure R., Grimme S., 2013, J. Comp. Chem., 34, 1672

Taquet V., Wirström E. S., Charnley S. B., 2016, ApJ, 821, 46

Tatewaki H., Huzinaga S., 1980, J. Comp. Chem., 1, 205

VandeVondele J., Hutter J., 2007, J. Chem. Phys., 127, 114105

Vasyunin A. I., Caselli P., Dulieu F., Jiménez-Serra I., 2017, ApJ, 842, 33

Vazart F., Ceccarelli C., Balucani N., Bianchi E., Skouteris D., 2020, MNRAS, 499, 5547

Vilela Oliveira D., Laun J., Peintinger M. F., Bredow T., 2019, J. Comp. Chem., 40, 2364

Wakelam V. et al., 2012, ApJS, 199, 21

Yabuta H., Williams L. B., Cody G. D., Alexander C. M. O. D., Pizzarello S., 2007, Meteorit. Planet. Sci., 42, 37

Yang Y.-L. et al., 2022, ApJ, 941, L13

Zamirri L., Casassa S., Rimola A., Segado-Centellas M., Ceccarelli C., Ugliengo P., 2018, MNRAS, 480, 1427

Zhao Y., Truhlar D. G., 2004, J. Phys. Chem. A, 108, 6908

Zhao Y., Truhlar D. G., 2008, Theor. Chem. Acc., 119 525

Zhao Y., Schultz N. E., Truhlar D. G., 2006, J. Chem. Theory Comput., 2, 364

APPENDIX A: BENCHMARK MODELS
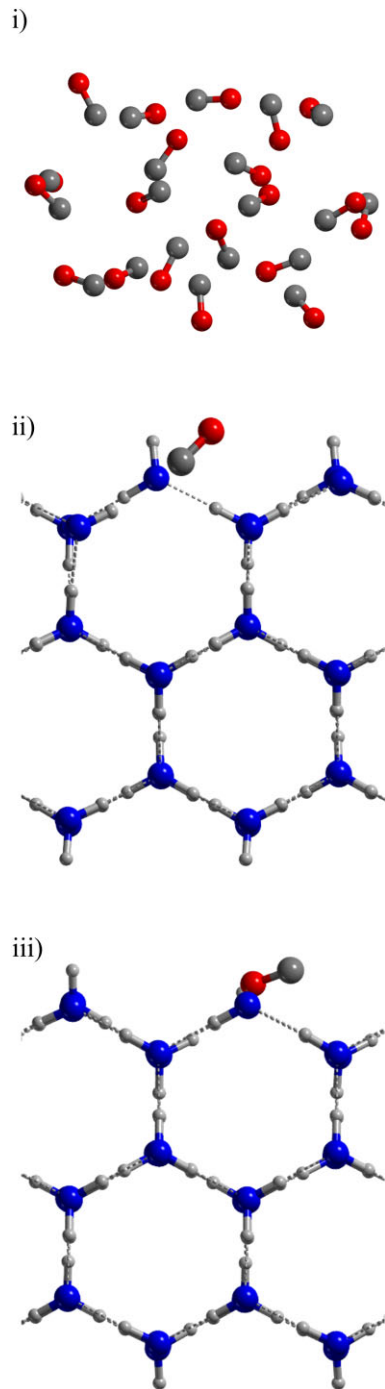
i)

ii)

iii)

Figure A1. Ice model used for the benchmark on the surface: (i) a cluster model made of 20 CO molecules, and the 2x1 supercell of (010) P-ice surface in which (ii) a water molecule exposing a dangling oxygen atom (H_2O Ice (a)) and (iii) a water molecule exposing a dangling hydrogen atom (H_2O Ice (b)) was substituted by a CO molecule.
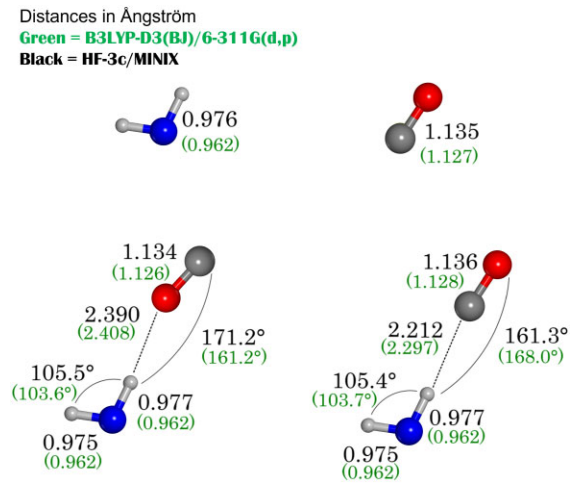
APPENDIX B: $H_2O \cdots CO$ INTERACTION

Figure B1. The interaction between CO and H_2O computed at HF-3c (black) and B3LYP-D3(BJ)/6-311G(d,p) (green) levels of theory. The H-bond established through the C-atom is energetically favoured over the one established through the O-atom of CO by only 0.3 kJ mol^{-1} at HF-3c level against 3.9 kJ mol^{-1} of B3LYP-D3(BJ).
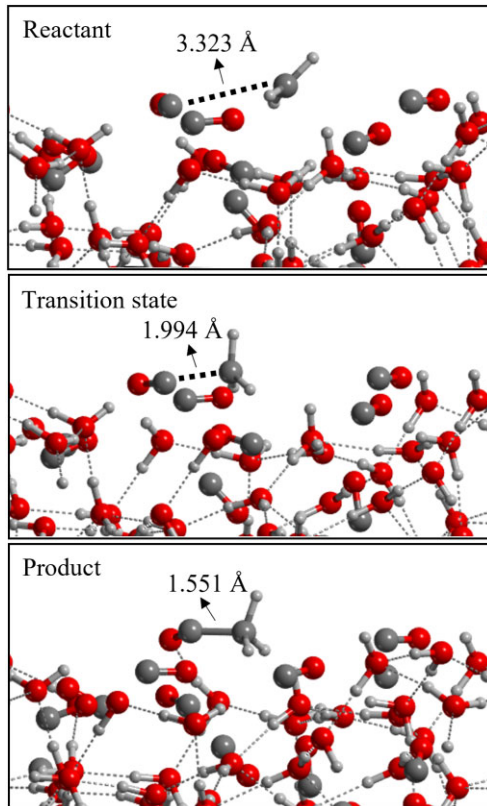
APPENDIX C: REACTION ON (100) SURFACE

Figure C1. Reactant, transition state, and product structures of the acetyl formation reaction on (100) surface, binding site **H1**. Colour code: H, white; C, grey; O, red.
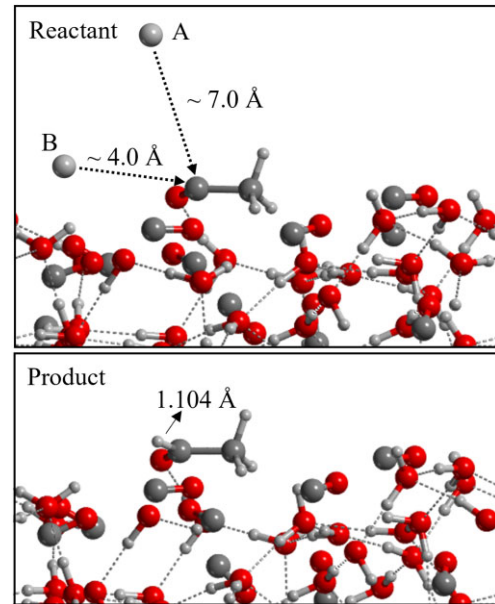

Figure C2. Reactants and product structures of the acetaldehyde formation reaction on (100) surface. The hydrogen atom approaching from the gas-phase (A) represents the Eley–Rideal mechanism, while in case of the Langmuir–Hinshelwood mechanism, the atom is adsorbed on the surface (B). Colour code: H, white; C, grey; O, red.

This paper has been typeset from a TEX/LATEX file prepared by the author.